Metabolic Characterization of Human Prostate Cancer with Tissue Magnetic Resonance Spectroscopy

Leo L. Cheng,[1,2] Melissa A. Burns,[1] Jennifer L. Taylor,[1] Wenlei He,[1,3] Elkan F. Halpern,[2] W. Scott McDougal,[3] and Chin-Lee Wu[1,3]

Departments of [1]Pathology, [2]Radiology, and [3]Urology, Massachusetts General Hospital, Harvard Medical School, Boston, Massachusetts

Abstract

Diagnostic advancements for prostate cancer have so greatly increased early detections that hope abounds for improved patient outcomes. However, histopathology, which guides treatment, often subcategorizes aggressiveness insufficiently among moderately differentiated Gleason score (6 and 7) tumors (>70% of new cases). Here, we test the diagnostic capability of prostate metabolite profiles measured with intact tissue magnetic resonance spectroscopy and the sensitivity of local prostate metabolites in predicting prostate cancer status. Prostate tissue samples (n = 199) obtained from 82 prostate cancer patients after prostatectomy were analyzed with high-resolution magic angle spinning proton magnetic resonance spectroscopy, and afterwards with quantitative pathology. Metabolite profiles obtained from principal component analysis of magnetic resonance spectroscopy were correlated with pathologic quantitative findings by using linear regression analysis and evaluated against patient pathologic statuses by using ANOVA. Paired t tests show that tissue metabolite profiles can differentiate malignant from benign samples obtained from the same patient (P < 0.005) and correlate with patient serum prostate-specific antigen levels (P < 0.006). Furthermore, metabolite profiles obtained from histologically benign tissue samples of Gleason score 6 and 7 prostates can delineate a subset of less aggressive tumors (P < 0.008) and predict tumor perineural invasion within the subset (P < 0.03). These results indicate that magnetic resonance spectroscopy metabolite profiles of biopsy tissues may help direct treatment plans by assessing prostate cancer pathologic stage and aggressiveness, which at present can be histopathologically determined only after prostatectomy. (Cancer Res 2005; 65(8): 3030-4)

Introduction

Prostate-specific antigen screening has effectively increased detection of prostate cancer at early stages. However, histopathology cannot reliably direct treatment in the prostate-specific antigen testing era: more than 70% of the newly diagnosed tumors receive a Gleason score (GS) of 6 or 7, yet clinical outcomes for these patients differ markedly (1). The limited prognostic insight of such clinical measures as prostate-specific antigen, Gleason score, and digital rectal exams often occasions either unnecessarily aggressive or dangerously conservative interventions (2–7). Prostate tumor heterogeneity further compromises histopathology in comprehensive evaluations as prostate cancer cells often elude biopsy, producing false negatives (8–10). More reliable and informative prognostic tools are needed. Changes in tumor metabolism, downstream from genomic and proteomic transformations, are thought to reflect disease-related biochemical reactivity, to precede histologically observable changes in cell morphology, and thus to offer an early means for predicting tumor behaviors (11).

Recently, high-resolution magic angle spinning proton magnetic resonance spectroscopy was developed for intact tissue analysis (12, 13). Magic angle spinning, originally used to reduce resonance line width in solid-state nuclear magnetic resonance, subjects samples to mechanical rotations (approximately in kilohertz) at the magic angle (54 degrees 44 minutes) away from the direction of the static magnetic field of the spectrometer while spectroscopy is recorded. Applied to intact tissues, high-resolution magic angle spinning can produce highly resolved spectra, allowing identification of individual metabolites while preserving tissue pathologic morphology.

We evaluated the diagnostic utility of prostate tissue metabolite profiles measured with high-field (14.1 T), high-resolution magic angle spinning proton magnetic resonance spectroscopy. Unaltered prostatectomy samples were analyzed spectroscopically, then histopathologically. Prostate metabolite profiles obtained from principal component analysis of tissue spectra were correlated with pathology quantities and with patient serum prostate-specific antigen levels. Finally, the diagnostic potentials of tissue metabolite profiles in predicting pathologic stage and tumor perineural invasion were investigated.

Materials and Methods

Sample collection. This study of human prostate tissue with magnetic resonance spectroscopy was reviewed and approved by the Institutional Review Board at Massachusetts General Hospital. Samples (n = 199, from 82 cancer prostatectomies) were collected from different prostate zones of the following patient population: (A) Gleason score: 5 [2 cases, 5 samples]; 6 [51, 126]; 7 [21, 53]; 8 [4, 9]; and 9 [4, 6]; and (B) American Joint Committee on Cancer/Tumor-Node-Metastasis (AJCC/TNM) stages (6th ed.): T_{2ab} [24 cases, 59 samples], T_{2c} [44, 112], T_{3a} [10, 17], T_{3b} [3, 5], and T_{3ab} [1, 6]. The few T_{3a}, T_{3b}, and T_{3ab} cases identified were combined and regarded in the study as T_3. Surgical tissue samples were snap frozen in liquid nitrogen and stored at −80°C until magnetic resonance spectroscopy. Patient clinical statuses were obtained from pathology reports.

High-resolution magic angle spinning proton magnetic resonance spectroscopy. A Bruker (Billerica, MA) AVANCE spectrometer operating at 600 MHz (14.1 T) was used for all magnetic resonance experiments. Tissue samples were placed into a 4-mm rotor with 10-μL plastic inserts. One-microliter D_2O was added for field locking. Spectra were recorded at 3°C with the spectrometer frequency set on the water resonance and a rotor-synchronized DANTE experimental protocol was applied with spinning at 600 and 700 Hz (±1.0 Hz; ref. 14). Thirty-two transients were averaged at a repetition time of 5 seconds.

Spectra were processed with AcornNMR-Nuts (Livermore, CA) according to the following procedures: 0.5-Hz apodization before Fourier

Requests for reprints: Leo L. Cheng, Pathology Research CNY-7, 149 13th Street, Charlestown, MA 02129. Phone: 617-724-6593; Fax: 617-726-5684; E-mail: cheng@nmr.mgh.harvard.edu.

transformation, baseline correction, and phase adjustment. Resonance intensities used in the study were integrals of curve fittings with Lorentzian-Gaussian line shapes measured from either 600- or 700-Hz high-resolution magic angle spinning spectrum (14).

Quantitative histopathology. Following spectroscopy, samples were fixed in 10% formalin, embedded in paraffin, cut into 5-μm sections at 100-μm intervals throughout the entire sample, and stained with H&E.

An Olympus BX41 Microscope Imaging System (Melville, NY), in conjunction with the image analyzer SoftImaging-MicroSuite (Lakewood, CO), was used to quantify sample cross sections. A pathologist with no knowledge of the spectroscopic results visually estimated to the nearest 5% the percent area representing cancer cells, normal epithelial cells, and stroma in each cross section. The percent volume of these features was calculated from the sizes of the cross sections and the corresponding percent area of each pathologic feature.

Statistical analysis. The aim of the present work was to correlate spectral metabolite profiles with tissue pathologies and patient clinical statuses. Prior to investigating such correlations, the metabolite matrix was subjected to statistical data treatment—principal component analysis—to reduce the complexity of spectral data.

Because certain pathologic processes can manifest simultaneous changes in multiple measurable metabolites, a change in a single metabolite may not represent the underlying process. Principal component analysis attempts to identify combinations (principal components) of the measured concentrations that may reflect distinct pathologic processes if they exist in the set of the samples. A positive contribution of a certain metabolite indicates the elevation of the metabolite within the component (process), and a negative contribution suggests suppression.

The components are ordered by the extent to which they are associated with variability in the observed cases. The more metabolites affected by a process (the more associated with a principal component), the greater the association. The stronger the change in the metabolites caused by a process, the greater the association. Additionally, the incidence of the process is a factor in the associated variability: extremely rare and extremely common processes cause little variability whereas processes that are seen in 50% of the cases have the greatest associated variability.

Principal components may differ from the actual underlying processes in one important respect. Principal components are required to be independent. Actual processes may affect some metabolites in common. For instance, one process might elevate metabolites A, B, C, and D, while suppressing E and F. A second process might elevate A and B, while suppressing C, D, E, and F. As both affect A, B, E and F in the same way, it is likely that the principal component analysis results identify a strong component, expressing an elevation of A and B with the simultaneous suppression of E and F. Another, possibly weaker, component might express metabolites C and D and would distinguish the first process from the second.

The hypothesis that different prostate pathologic features (percent volume epithelia, cancer cells, stroma) possess different metabolite profiles can thus be tested by using linear regression analysis against these principal components. Paired Student's t tests were used to evaluate the ability of cancer-related principal component 13 and its major contributing metabolites (phosphocholine and choline) to differentiate cancerous from histologically benign samples obtained from the same patient, whereas discriminant analyses were used to generate a canonical plot to achieve the maximum separation between the two groups, with accuracy being analyzed by receiver operating characteristic curves (15). Student's t tests were used

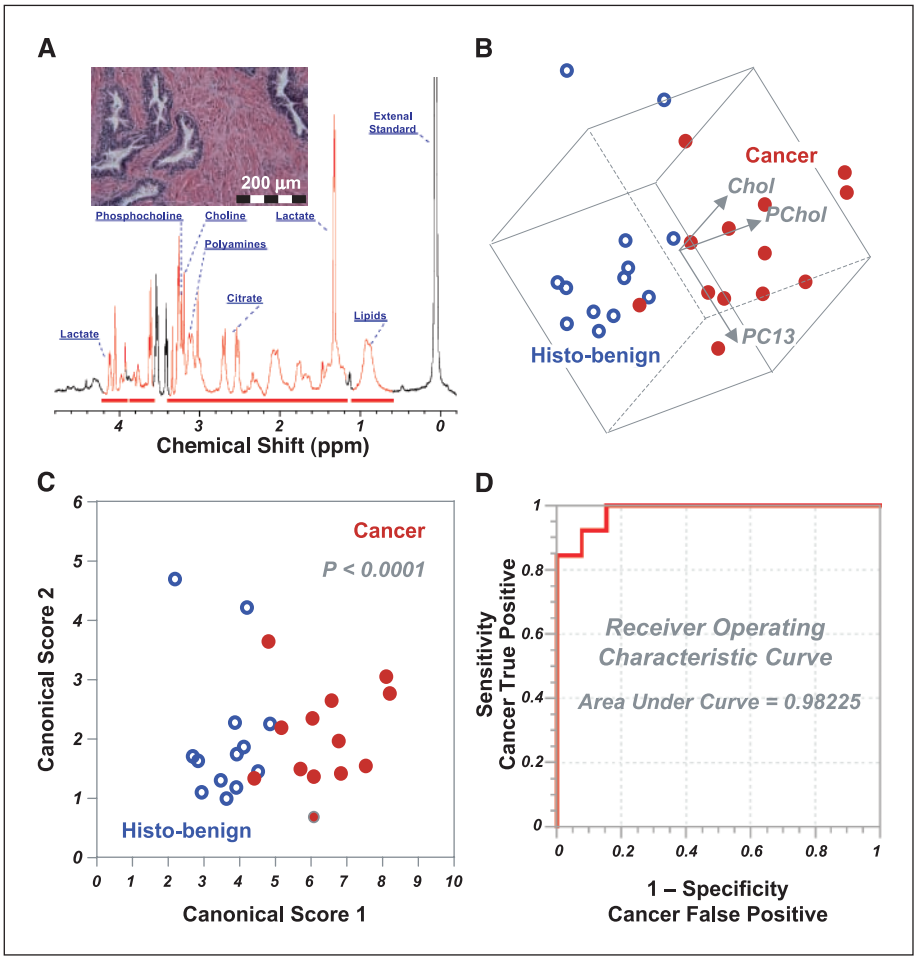

Figure 1. *A*, high-resolution magic angle spinning ^{1}H MR spectrum of intact tissue obtained from the removed prostate of a 61-year-old patient with GS 6 T_{2b} tumors. Histopathology analysis of the tissue sample (*insert*) after its spectroscopy measurement revealed that the sample contained 40% histopathologically defined benign epithelium and 60% stromal structures, with no identifiable cancerous glands. Cellular metabolites mentioned in the text are labeled on the spectrum. The 36 most intense resonance peaks or metabolite groups above the horizontal bars were selected for analyses, whereas the other regions were excluded from calculation, partly due to surgery-related alcohol contamination. *B*, three-dimensional plot of principal component 13 (PC13 correlates linearly with percent volume of cancer cells in tissue samples) versus phosphocholine versus choline. Cancerous and histologically benign (histo-benign) tissue samples from 13 patients can be visually separated in observation plane. The paired Student's t test results (cancer versus histo-benign from the same patients) for principal component 13, phosphocholine, and choline are 0.012, 0.004, and 0.001. Only results from these 13 patients could be evaluated with paired tests for other cancer positive samples were collected from patients from whom no histo-benign samples were analyzed. *C*, the canonical plot resulting from discriminant analysis of the three variables in *B* presents the maximum separation between the two groups. *D*, the resulting receiver operating characteristic curves indicates the accuracy of using the three variables in *B* to positively identify cancer samples.

to investigate the relationship between cancer-related principal component 14 and tumor perineural invasion. The abilities of principal components 2 and 5 to differentiate between pathologic stages were tested using ANOVA. Statistical analyses were carried out using SAS-JMP (Cary, NC).

Results and Discussion

High-resolution tissue proton magnetic resonance spectroscopy and principal component analysis. High-resolution magic angle spinning magnetic resonance spectroscopy permits the acquisition of high-resolution proton spectra from intact tissue, while preserving tissue architectures for subsequent histopathologic analysis (Fig. 1*A*). To achieve high resolution before high-resolution magic angle spinning, tissue metabolites were analyzed in solutions of chemical extraction so that results depended on the applied procedures and their completeness. Furthermore, tumor heterogeneity limits the usefulness of extraction approaches.

Histomorphologic evaluations proved critical for the correct interpretation of spectroscopic data obtained from the same samples. In this study, 20 of 199 analyzed samples from prostate cancer patients contained cancerous glands, whereas the rest (n = 179) represented histologically benign tissue obtained from cancerous prostates. This frequency reflects the infiltrative, heterogeneous nature of prostate cancer; producing no visible mass, its architecture precludes cancer-selective tissue removal and thus accounts for the clinical complexity of prostate biopsy (8–10).

Principal component analysis was carried out on the concentrations of the 36 most intense resonance peaks or groups assigned to specific metabolites to generate principal components representing different variations of tissue metabolite profiles. Because of the existence of pathologic variations among the samples, certain principal components may capture these variations. For instance, principal component 2, reflecting changes in polyamines, citrate, etc., was found to differentiate epithelia from stroma with statistical significance (16.5% of variance; epithelia: r = 0.381, P < 0.0001; stroma: r = −0.303, P < 0.0001), in agreement with previous observation (16). Moreover, both principal component 13 and principal component 14 differentiate cancer from stroma (cf. principal component 14 represents 1.54% of variance; cancer: r = −0.160, P = 0.0243; stroma: r = 0.217, P = 0.0021). The difference of variance representation (16.5% versus 1.54% of the total variability of the standardized 36 metabolites for principal components 2 and 14, respectively) agrees with the fact that only 10% of the samples were identified as cancer positive, whereas >90% of them were designated epithelium positive. Of note, not all principal components are related with the evaluated pathologies. Many of them may indicate intrinsic differences that are not evaluated or variables, such as spectrometer instabilities, that are not the subjects of interest.

Differentiating cancer from histologically benign samples. By using histologically defined noncancer (histo-benign) samples from 13 of 20 patients from whom histologically cancer-positive samples were also analyzed, we observed a separation between the cancerous and histo-benign groups on a plane of a three-dimensional plot (Fig. 1*B*) of principal component 13 versus phosphocholine and choline. Both metabolites were found to be the major contributors to principal components 13 and 14, in agreement with descriptions by the current *in vivo* and *ex vivo* magnetic resonance spectroscopy literature of their relationship with malignancy (18). Further, both principal components were linearly correlated (P: 0.04, 0.02) with percent volume of cancer cells. Application of discriminant analysis to the three variables indicated a classification accuracy of 92.3% (Fig. 1*C*). An overall accuracy of 98.2% for the identification of cancer samples was obtained from a receiver operating characteristic curve generated from the three variables (Fig. 1*D*).

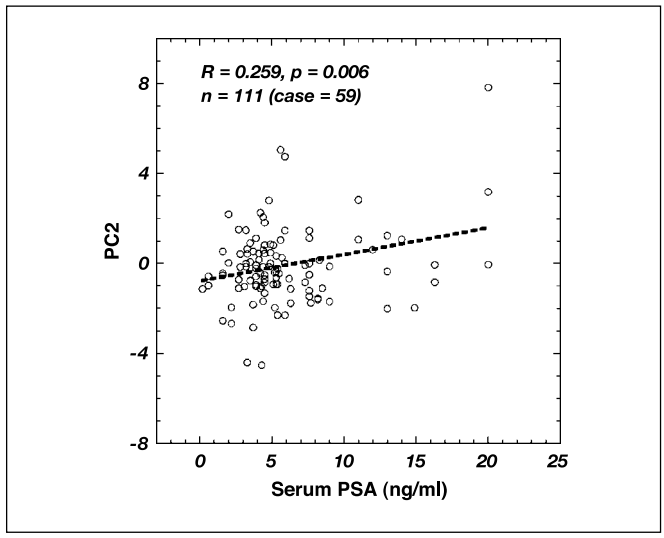

Figure 2. Statistically significant correlation between the patient serum prostate-specific antigen levels before prostatectomy and the metabolite profiles represented by principal component 2 (*PC2*), as measured from 111 histo-benign prostate tissue samples obtained from 59 prostatectomy cases for prostate cancer. Plotted principal component 2 values represent the linear combinations of metabolite concentrations according to the principal component 2 formula obtained from principal component analysis.

Correlating with patient serum prostate-specific antigen levels. From the 82 prostatectomy cases studied, we identified 59 cases for which the serum prostate-specific antigen levels of patients before surgery were available. Among these, 111 histo-benign tissue samples from different prostate zones (central, transitional, and peripheral) were identified. We evaluated the relationship between prostate-specific antigen levels and tissue metabolite profiles, and found that principal component 2 was linearly correlated, with statistical significance, to prostate-specific antigen results (Fig. 2). Because principal component 2 is linearly correlated with the percent volume of histo-benign epithelial cells, as previously presented, we verified that no coincidental correlation occurred between prostate-specific antigen levels and epithelial percent volume among these measured samples.

Identifying tumor pathologic stages and predicting tumor perineural invasion. We examined the correlation between principal components and tumor pathologic stage (AJCC/TNM staging system). With all 199 samples, we observed that principal component 2 differentiated T_{2c} cancer (prostate-confined; both lobes) from T_3 (invading extraprostatic tissue, P < 0.03) and T_{2ab} cancer (prostate confined; one lobe, P < 0.005). Principal component 5 also differentiated T_{2ab} cancer from T_{2c} (P < 0.003) and T_3 cancer (P < 0.00005). Again, we verified that the observed principal component 2 differentiation among tumor stages was independent of epithelial content (e.g., T_{2ab}, 21.88 ± 2.59%; T_{2c}, 20.21 ± 1.91%).

More interestingly, on analysis of the histo-benign samples (n = 179), similar differentiations persisted for both principal

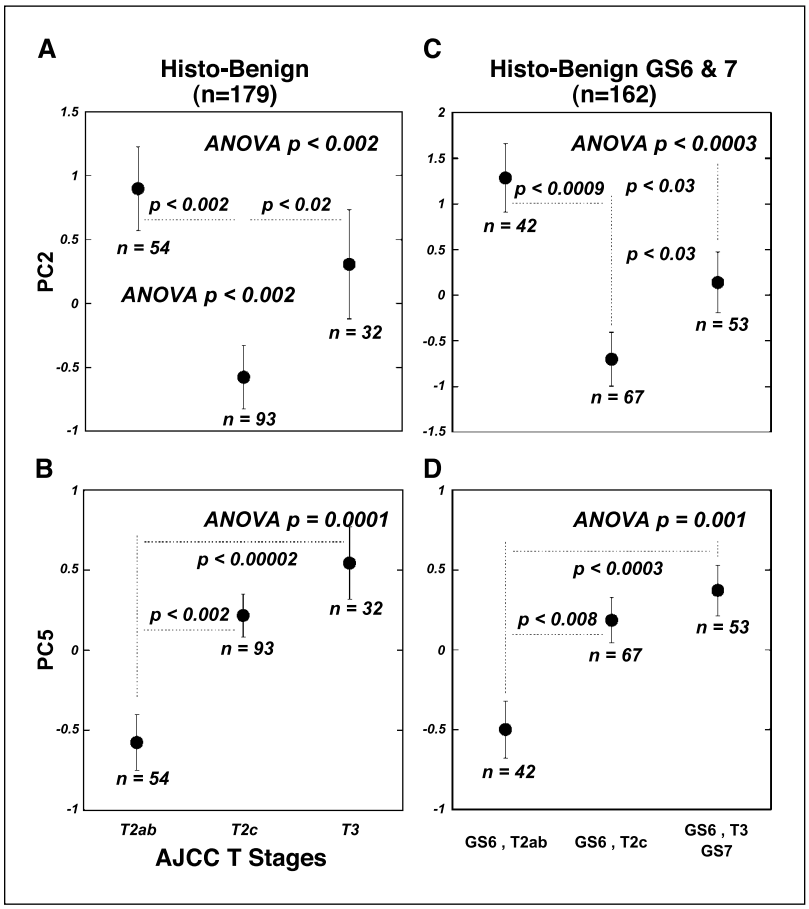

Figure 3. Principal components 2 and 5 as predictors of tumor stage. Principal component 2 (*A*) can differentiate T_{2c} stage tumors from T_{2ab} and T_3 tumors, whereas principal component 5 (*B*) can differentiate T_{2ab} from T_{2c} and T_3 stages, as defined by AJCC/TNM staging system with histo-benign samples, and with histo-benign GS 6 and 7 samples (*C* and *D*). In the latter, principal components 2 and 5 can differentiate among three tumor groups: GS 6 T_{2ab}, GS 6 T_{2c}, and GS 6 T_3 plus GS 7 tumors.

components (Fig. 3*A* and *B*). Furthermore, when the same principal components were applied to histo-benign samples of GS 6 and 7 tumors (n = 162), both principal components identified the least aggressive tumor (i.e., GS 6 T_{2ab} tumors, n = 42) from those of the more aggressive groups (GS 6 T_{2c}, GS 6 T_3, and GS 7 tumors; Fig. 3*C* and *D*).

Tumor perineural invasion status, although not yet incorporated in AJCC/TMN staging, indicates prostate tumor aggressiveness and aids treatment planning (17). Unfortunately, tumor heterogeneity prevents the visualization of invasion in biopsy samples. Our evaluation yielded a statistically significant correlation between principal component 14 levels and invasion status for all 199 samples (126 "+" and 73 "−"; $P < 0.01$), for 179 histo-benign samples (103 "+" and 71 "−"; $P < 0.035$), and more interestingly, for 42 histo-benign samples from GS 6 T_{2ab} tumors (13 "+" and 29 "−"; $P < 0.028$). This last observation, combined with results shown in Fig. 3*E* and *F*, may have great clinical significance in identifying and managing the less aggressive tumor group within the >70% newly diagnosed moderately differentiated tumors.

Our findings, with respect to tumor pathologic stages and perineural invasion, present an important indication of the technique's potential to improve current pathology in prostate cancer diagnosis. Despite its significance in treatment planning, tumor pathologic stage can now only be assessed from resected prostate. Our observations indicate that metabolite profiles may provide a "second opinion" for prostate biopsy evaluation. They further suggest that an additional biopsy core, obtained to generate metabolite profiles, could help predict tumor stage for cancer-positive patients, even if the core itself is histo-benign.

In this report, we emphasize the phrase "histo-benign" to introduce the fact that the noncancer status of these tissue samples was based on histologic examination. We also emphasize that currently our metabolite results are analyzed according to histopathology, which remains the "gold standard" for cancer diagnosis and treatment planning. However, evaluation of the metabolite paradigm presented, and its usefulness in the oncology clinic, may require reconsideration of the boundaries of histopathology and metabolites. Current wisdom concerning the development and progression of malignancy, such as the widely proposed stroma effects, may assist this transformation (19, 20).

Our data leave unanswered questions. First, we cannot be certain from where, in proximity to cancer glands, our histo-benign samples were obtained. Therefore, we cannot predict whether observed metabolite alterations are global or focal. Additionally, comparisons between cancer-positive and histo-benign samples rely entirely on tissue from prostate cancer patients due to the lack of normal controls and the disqualifying metabolic degradation of tissue upon death. Our limited number of cancer-positive samples has also prevented determination of prostate pathologic stage based exclusively on cancer-positive samples.

We have nevertheless shown that metabolites measured with tissue magnetic resonance spectroscopy correlate with histopathology findings and that metabolite profiles reveal overall tumor clinicopathologic status and aggressiveness before either is

visible to histopathology. We believe the data presented here show the diagnostic and prognostic potential of the metabolite protocol. However, its clinical utility can be assessed only through longitudinal patient follow-up. Only correlations between tumor metabolites and patient outcome will allow us to establish the sensitivity and specificity of diagnostic and prognostic values for tumor metabolites, independent of current pathology.

Acknowledgments

Received 11/16/2004; revised 2/4/2005; accepted 2/16/2005.

Grant support: Public Health Service/NIH grants CA80901, CA095624, and EB002026, and DOD grant W81XWH-04-1-0190.

The costs of publication of this article were defrayed in part by the payment of page charges. This article must therefore be hereby marked *advertisement* in accordance with 18 U.S.C. Section 1734 solely to indicate this fact.

We thank Dr. Kurt J. Isselbacher for encouragement, guidance, and support.

References

1. Pound CR, Partin AW, Eisenberger MA, Chan DW, Pearson JD, Walsh PC. Natural history of progression after PSA elevation following radical prostatectomy. Jama 1999;281:1591–7.
2. Carter HB, Isaacs WB. Improved biomarkers for prostate cancer: a definite need. J Natl Cancer Inst 2004;96:813–5.
3. Incrocci L, Slob AK. Incidence, etiology, and therapy for erectile dysfunction after external beam radiotherapy for prostate cancer. Urology 2002;60:1–7.
4. Eton DT, Lepore SJ. Prostate cancer and health-related quality of life: a review of the literature. Psychooncology 2002;11:307–26.
5. Ko YJ, Bubley GJ. Prostate cancer in the older man. Oncology (Huntingt) 2001;15:1113–9, 23–4; discussion 24–6, 31.
6. Ransohoff DF, McNaughton Collins M, Fowler FJ. Why is prostate cancer screening so common when the evidence is so uncertain? A system without negative feedback. Am J Med 2002;113:663–7.
7. Smith RA, Cokkinides V, Eyre HJ. American Cancer Society guidelines for the early detection of cancer, 2003. CA Cancer J Clin 2003;53:27–43.
8. Zackrisson B, Aus G, Lilja H, Lodding P, Pihl CG, Hugosson J. Follow-up of men with elevated prostate-specific antigen and one set of benign biopsies at prostate cancer screening. Eur Urol 2003;43:327–32.
9. Mazal PR, Haitel A, Windischberger C, et al. Spatial distribution of prostate cancers undetected on initial needle biopsies. Eur Urol 2001;39:662–8.
10. Steiner H, Moser P, Hager M, et al. Clinical and pathologic features of prostate cancer detected after repeat false-negative biopsy in a screening population. Prostate 2004;58:277–82.
11. Mountford C, Doran S, Lean C, Russell P. Cancer pathology in the year 2000. Biophys Chem 1997;68:127–35.
12. Cheng LL, Lean CL, Bogdanova A, et al. Enhanced resolution of proton NMR spectra of malignant lymph nodes using magic-angle spinning. Magn Reson Med 1996;36:653–8.
13. Cheng LL, Ma MJ, Becerra L, et al. Quantitative neuropathology by high resolution magic angle spinning proton magnetic resonance spectroscopy. Proc Natl Acad Sci U S A 1997;94:6408–13.
14. Taylor JL, Wu CL, Cory D, Gonzalez RG, Bielecki A, Cheng LL. High-resolution magic angle spinning proton NMR analysis of human prostate tissue with slow spinning rates. Magn Reson Med 2003;50:627–32.
15. McNeil BJ, Keller E, Adelstein SJ. Primer on certain elements of medical decision making. N Engl J Med 1975;293:211–5.
16. Cheng LL, Wu C, Smith MR, Gonzalez RG. Non-destructive quantitation of spermine in human prostate tissue samples using HRMAS ^{1}H NMR spectroscopy at 9.4 T. FEBS Lett 2001;494:112–6.
17. Beard CJ, Chen MH, Cote K, et al. Perineural invasion is associated with increased relapse after external beam radiotherapy for men with low-risk prostate cancer and may be a marker for occult, high-grade cancer. Int J Radiat Oncol Biol Phys 2004;58:19–24.
18. Podo F. Tumour phospholipid metabolism. NMR Biomed 1999;12:413–39.
19. Wong YC, Wang XH, Ling MT. Prostate development and carcinogenesis. Int Rev Cytol 2003;227:65–130.
20. Cooper CR, Chay CH, Gendernalik JD, et al. Stromal factors involved in prostate carcinoma metastasis to bone. Cancer 2003;97:739–47.